Mossbauer-effect study of the hyperfine field distributions in the residual amorphous phase of Fe-Cu-Nb-Si-B nanocrystalline alloys

1994 J. Phys.: Condens. Matter 6 1431

(http://iopscience.iop.org/0953-8984/6/7/015)

J. Phys.: Condens. Matter 6 (1994) 1431–1438. Printed in the UK

Mössbauer-effect study of the hyperfine field distributions in the residual amorphous phase of Fe–Cu–Nb–Si–B nanocrystalline alloys

Marcel Miglierini

Department of Nuclear Physics and Technology, Slovak Technical University, Ilkovičova 3, 812 19 Bratislava, Slovakia

Received 13 September 1993, in final form 26 October 1993

Abstract. Amorphous $Fe_{73.5-x}Cu_1Nb_{3+x}Si_{13.5}B_9$ ($x = 0$ and 1.5) alloys were isothermally heat treated at 550° C in a vacuum for up to 16 h. ^{57}Fe transmission Mössbauer spectra revealed a lower rate of crystallization for $x = 1.5$. The annealing time dependences of the hyperfine parameters and the different behaviours of the intergranular component in both samples were studied via three-dimensional projections of the hyperfine field distributions. Segregation of Fe, Si and also B, from which the crystalline phases have been created, lead to a depletion of these elements in the residual amorphous phase. As a consequence, the number of Fe atoms with Nb, Cu and possibly B atoms in their nearest surroundings increased, giving rise to changes in the chemical and topological short-range order. The amount of the residual amorphous phase as well as its average hyperfine field decreased whereas the standard deviation of the hyperfine field distribution increased with increasing annealing time.

1. Introduction

The nanocrystalline structure which substantially improves the magnetic properties of Fe–Cu–Nb–Si–B-type alloys [1] is attracting much interest at present. One way of obtaining nanometre-order grains requires the use of precursor, i.e. an amorphous metal quenched from the melt which is suitably heat treated [2]. Identification of iron-containing phases which are created during annealing as well as elucidation of their structural and magnetic properties are effectively performed by Mössbauer spectroscopy [3]. Using this technique, the crystallization kinetics of the $Fe_{73.5}Cu_1Nb_3Si_{13.5}B_9$ alloy have been widely studied [4–7]. Different compositions of the Fe–Cu–Nb–Si–B system have also been examined by Mössbauer effect measurements [3, 8–10]. The influence of Nb substitution by Mo, W or Zr [11] and Cu by Au, Ag, Pd, Pt or Mn [12] on the fine-grain structure formation was also investigated. The role of particular components during crystallization and the behaviour of the amorphous residual phase, however, are not yet fully understood.

Unlike the previous papers [3–7], which concentrated on the phase analysis of the nanocrystalline $Fe_{73.5}Cu_1Nb_3Si_{13.5}B_9$ alloy, here the main emphasis is the changes in the hyperfine field distributions, yielding information about the short-range order of the residual amorphous phase. The time-dependent behaviour of the distributions is documented with the help of their three-dimensional (3D) projections. The present work also deals with the influence of a different Fe-to-Nb ratio on the crystallization kinetics of the master Fe–Cu–Nb–Si–B alloy.

0953-8984/94/071431+08$07.50

2. Experimental details

Amorphous $Fe_{73.5-x}Cu_1Nb_{3+x}Si_{13.5}B_9$ ($x = 0$ and 1.5) ribbons (width, 10 mm; thickness, 23 μm and 24 μm, respectively) have been prepared by the method of planar flow casting at the Institute of Physics, Slovak Academy of Sciences, Bratislava. Pieces about 2 cm long were isothermally annealed at 550 °C in a vacuum furnace ($p \sim 10^{-3}$ Pa) for up to 16 h.

Transmission ^{57}Fe Mössbauer spectra, all taken at room temperature, were collected with a conventional constant-acceleration spectrometer using a ^{57}Co(Rh) source. They were evaluated by the NORMOS DIST program [13] which allows simultaneous treatment of both distribution and discrete values of hyperfine magnetic fields. Calibration was carried out using a 25 μm α-Fe foil. Details of the fitting models are given below.

3. Results and discussion

3.1. Fitting models

Six-line patterns of broad and overlapped absorption dips which represent a variety of structurally inequivalent Fe sites in the amorphous samples were analysed using the distributions $P(H)$ of the hyperfine magnetic fields. Asymmetries in the spectrum line intensities were accounted for by introducing a linear correlation between the isomer shifts and the hyperfine fields for all components of the distributions. The relative area D_{23}, of lines 2 and 5 with respect to lines 3 and 4 was fitted and the relative area D_{13} of lines 1 and 6, was fixed at a value of 3 (table 1).

Table 1. Hyperfine parameters obtained from the Mössbauer spectra of the as-quenched $Fe_{73.5-x}Cu_1Nb_{3+x}Si_{13.5}B_9$ alloy.

$x = 0$			$x = 1.5$		
$\langle H \rangle$ (T)	σ_H (T)	D_{23}	$\langle H \rangle$ (T)	σ_H (T)	D_{23}
20.66	4.76	2.38	18.63	5.13	1.85

Annealing of the amorphous ribbon at 550 °C led to the formation of nanocrystalline grains [14]. As a consequence, sharp and isolated lines emerged in the Mössbauer spectra. In the fitting model we have used six sextets of Lorentzian lines in addition to one distributed sextet. The former are intended to reproduce crystallographic sites whereas the latter belongs to the residual intergranular uncrystallized amorphous phase. The hyperfine parameters obtained from the Mössbauer spectra of both $x = 0$ and $x = 1.5$ samples annealed for 1 h are summarized in table 2.

The number of crystalline components which have been used in the literature to fit the Mössbauer spectra of nanocrystalline $Fe_{73.5}Cu_1Nb_3Si_{13.5}B_9$ varies from four [4–6] to six [7] and seven [3] considering only the $D0_3$ structure of Fe_3Si, iron–silicon compounds and also the presence of iron–boron phases, respectively. We ascribed five sextets (denoted as c1–c3, c5 and c6) to the Fe–Si phases and two sextets (c4 and c5) to boride-like Fe sites. Similar to [3], an overlap of one Fe–B and Fe–Si sextet is assumed in c5. The amount of borides in the samples is so small that the third sextet ($H \simeq 22$ T from [3]) was not seen.

The uncrystallized intergranular phase was fitted by one broadened sextet of Lorentzian lines in [4] and [5]. Rixecker *et al* [7] adopted a sextet of pseudo-Lorentzian profiles

Table 2. Hyperfine parameters obtained from the Mössbauer spectra of the $Fe_{73.5-x}Cu_1Nb_{3+x}Si_{13.5}B_9$ alloy annealed at 550 °C for 1 h in vacuum.

	$x = 0$			$x = 1.5$		
	H (T)	FWHM (mm s^{-1})	A_{rel} (%)	H (T)	FWHM (mm s^{-1})	A_{rel} (%)
AM	18.9[a]	6.06[b]	57.8	18.5[a]	5.65[b]	92.3
c1	32.13	0.33	9.0	32.11	0.27	1.3
c2	30.69	0.32	6.5	30.96	0.27	1.4
c3	28.88	0.27	2.9	29.05	0.28	0.7
c4	27.17	0.27	1.9	27.26	0.27	0.2
c5	24.66	0.35	10.0	24.59	0.33	2.0
c6	19.64	0.33	11.9	19.58	0.28	2.1

[a] Average hyperfine field of $P(H)$.
[b] Standard deviation of $P(H)$ in teslas.

for this purpose. Pundt *et al* [6] fitted the amorphous subspectrum by a data file which was obtained by measuring the Mössbauer spectrum of the as-quenched alloy at room temperature. The only fitted parameter was the relative area of this component. They represented each 'crystalline' subspectrum by a Zeeman split pattern using five Lorentzian sextets. Since one of these exhibited rather a large linewidth, Pundt *et al* [6] assigned it to a new 'emaciated' amorphous phase. Thus, they obtained two different amorphous phases in the annealed sample: the amorphous phase with a hyperfine field distribution the same as that of the as-quenched alloy and an 'emaciated' amorphous phase containing less Fe, Si and B and, probably, more Nb and Cu [6].

We found the interpretations of the residual amorphous phase by either one sextuplet of broadened lines [4, 5, 7] or consisting of two 'different' amorphous phases [6] unsuitable for the description of the short-range order. As in fully amorphous specimens, the residual uncrystallized phase in the annealed samples should be represented by a distribution of hyperfine fields [3, 10–12, 15, 16].

The intergranular component (denoted AM in table 2) was fitted by a distributed sextet. It is noteworthy that with respect to the original amorphous phase the average hyperfine field decreased but the standard deviation of $P(H)$ increased in both cases. A decrease in the average field of the residual amorphous phase was reported also in [3–7]. Both effects are due to changes in the short-range order which are taking place in the process of crystallization and they will be discussed in more detail later using 3D projections of the $P(H)$ distributions.

3.2. Mössbauer spectra

Time-dependent evolution of crystalline components in $Fe_{73.5-x}Cu_1Nb_{3+x}Si_{13.5}B_9$ annealed at 550 °C is demonstrated by means of the Mössbauer spectra in figures 1 and 2 for $x = 0$ and $x = 1.5$, respectively. An increase in the Nb content at the expense of Fe reduces the Fe-to-Nb ratio and, as a consequence, the onset of crystallization in the $x = 1.5$ sample is delayed.

The behaviour of the residual amorphous phase in the course of isothermal annealing can be seen from the parameters of the distributed components in figure 3. Relative area A_{rel}, of the distributed sextet in a Mössbauer spectrum is directly proportional to the amount of the intergranular phase in a specimen. The open circles in figure 3(*a*) show a steep decrease in the relative area for $x = 0$, which implies rapid crystallization of this sample. As for the

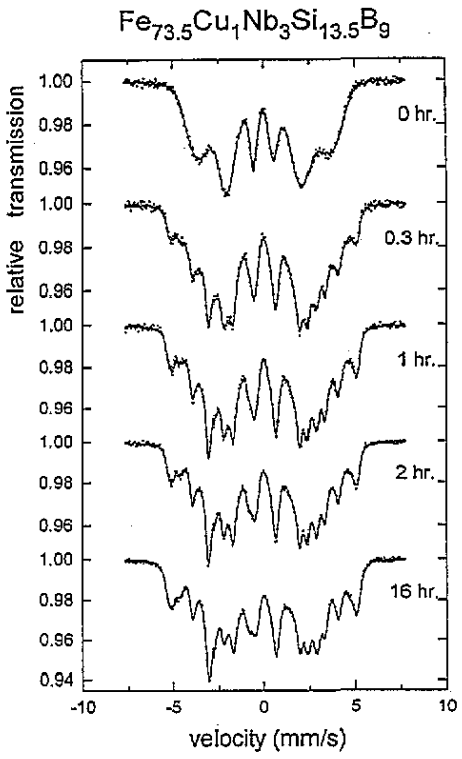

Figure 1. Room-temperature Mössbauer spectra of the $Fe_{73.5}Cu_1Nb_3Si_{13.5}B_9$ alloy taken after the indicated annealing times at 550° C in vacuum.

$x = 1.5$ sample, the higher Nb content causes a moderate decrease in the amount of the residual amorphous phase as shown by the full circles in figure 3(*a*). It can be concluded that the fine-grain structure formation in the $Fe_{73.5-x}Cu_1Nb_{3+x}Si_{13.5}B_9$ alloy can be reduced by increasing the fraction of Nb atoms.

The time dependences of the average fields, $\langle H \rangle$, are illustrated in figure 3(*b*). The sample with higher Nb content ($x = 1.5$) (full circles) depicts lower $\langle H \rangle$-values in the whole range of annealing times than does the $x = 0$ alloy (open circles). This can be explained by higher number of Fe atoms that have mostly Nb atoms as their nearest neighbours in the $x = 1.5$ sample.

The steep decrease in $\langle H \rangle$ for $x = 0$ (open circles in figure 3(*b*)) within the first 2 h of annealing is connected with rapid crystallization of this alloy, as mentioned above. Fast segregation of Fe and Si atoms from the original precursor quickly reduces the number of Fe atoms with higher hyperfine fields, and the Fe atoms with Cu, Nb and B in their local surroundings start to dominate. Consequently, the resulting hyperfine field is reduced.

The same mechanism can be used to interpret the decrease in $\langle H \rangle$ in the $x = 1.5$ sample in the course of annealing. The different character of the curve also suggests different crystallization kinetics for this alloy. The higher Nb content in the $x = 1.5$ sample causes changes in the magnetic structure of the as-cast amorphous specimens, too. They are demonstrated by the fall in the $\langle H \rangle$-value in table 1 with respect to the $x = 0$ sample as well as by the different orientations of the net magnetic moment. Taking the parameter D_{23} from table 1 into account, we conclude that for $x = 0$ the moments are oriented nearly

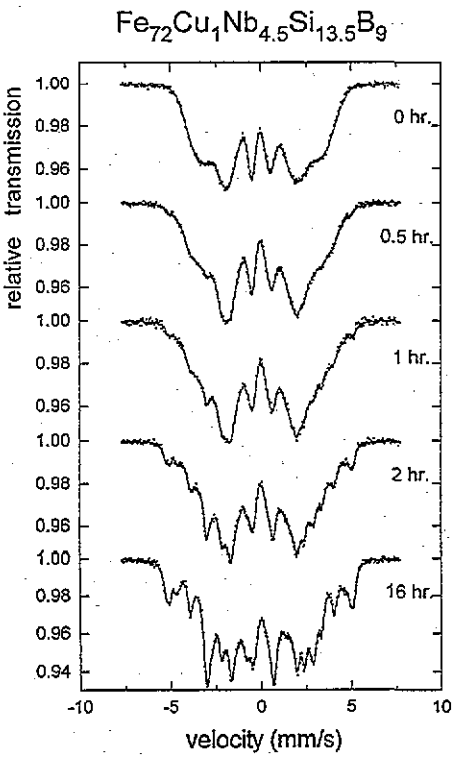

Figure 2. Room-temperature Mössbauer spectra of the $Fe_{72}Cu_1Nb_{4.5}Si_{13.5}B_9$ alloy taken after the indicated annealing times at 550 °C in vacuum.

randomly and those for $x = 1.5$ sample depict a tendency to turn out of the ribbon plane.

As for the samples annealed for 1 h the D_{23}-values of the residual amorphous phase are 2.65 and 3.23 for $x = 0$ and $x = 1.5$, respectively. In both cases an increase in D_{23} is observed with respect to those of the original as-quenched state. This can be associated with changes in the magnetic structure of the intergranular component which are both time and concentration dependent (see below). It should be noted that D_{23} for the crystalline components was fixed during the fitting procedure to the value of 2.8, as in [5, 6].

The increase in the standard deviations σ_H of the $P(H)$ distributions with increasing annealing time in figure 3(c) for both samples implies changes in the local short-range order. They are taking place during heat treatment when, owing to crystallization, the nominal composition of the constituent elements in the residual amorphous phase differs from that observed in the original as-quenched state. We discuss the changes in the local short-range order with the help of 3D projections of the $P(H)$ distributions in the next section.

3.3. Hyperfine field distributions

The hyperfine field distributions $P(H)$ provide direct information concerning the short-range order. To analyse the changes in the atomic arrangement of the residual amorphous phase with respect to the proceeding crystallization, i.e. annealing time, we adopted 3D projections of the corresponding distributions. They are shown in figures 4 and 5 for the $Fe_{73.5-x}Cu_1Nb_{3+x}Si_{13.5}B_9$ alloy with $x = 0$ and $x = 1.5$, respectively.

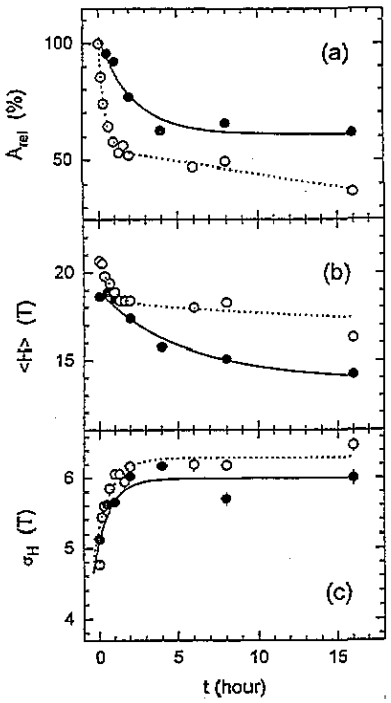

Figure 3. Parameters of the residual amorphous phase in the $Fe_{73.5-x}Cu_1Nb_{3+x}Si_{13.5}B_9$ alloy: (*a*) relative amount A_{rel}; (*b*) average hyperfine field, $\langle H \rangle$; (*c*) standard deviation σ_H of $P(H)$, plotted against the annealing time t for $x = 0$ (○) and $x = 1.5$ (●).

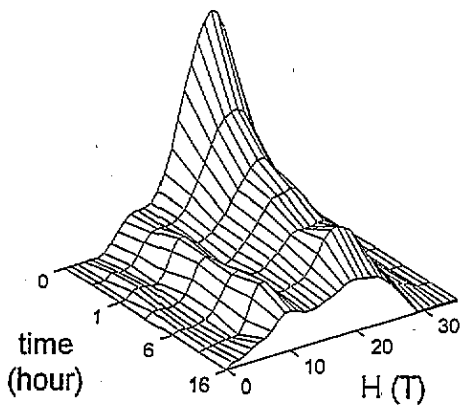

Figure 4. 3D projections of the hyperfine field distributions corresponding to the residual amorphous phase of the $Fe_{73.5}Cu_1Nb_3Si_{13.5}B_9$ alloy.

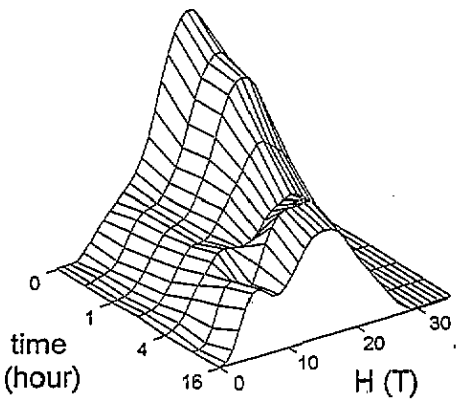

Figure 5. 3D projections of the hyperfine field distributions corresponding to the residual amorphous phase of the $Fe_{72}Cu_1Nb_{4.5}Si_{13.5}B_9$ alloy.

The field values on H are given on the abscissa and their probability values $P(H)$ on the z axis. Stacking the individual $P(H)$ with respect to the annealing time, we obtained the y axis of the 3D distribution. It should be noted that the time axes in figures 4 and 5 are not linear but nearly logarithmic.

3D projections exhibit complex information about changes in the short-range order according to the annealing time and field values. Choosing different viewpoints on the 3D graphs, we are able to inspect all $P(H)$-values. Thus, mutual correlation between the investigated parameters can be revealed.

We interpret the bimodal nature of the $P(H)$ that we obtained as due to the presence of two distinct types of resonant atom surroundings. High-field values can be associated with those Fe atoms which have primarily Si and B as nearest neighbours, whereas the low-field component is ascribed to the Fe atoms surrounded by Cu, Nb and also B. The average hyperfine field derived from the completely amorphous samples (see table 1) agrees reasonably well with the results of Zemčík [3] and Rixecker *et al* [7].

Zemčík [3] adopted two superimposed Gaussian distributions indicating two types of surroundings to model the distribution asymmetry. In the analysis of the as-cast samples, Rixecker *et al* [7] employed the program of LeCaër and Dubois [17] and obtained also bimodal $P(H)$.

Looking at figures 4 and 5 one can see two distinct humps which correspond to the bimodal nature of $P(H)$ as discussed above. Since both graphs are drawn on the same scale, the more pronounced decrease in the high-field hump in figure 4 suggests rather rapid crystallization in the $x = 0$ sample. The high-field hump represents those Fe atoms which are surrounded mostly by Si and B atoms, and these are the elements from which the crystalline phases have been formed. That is why it is not surprising that it is mainly the high-field hump that decreases during annealing, i.e. crystallization. This is also the origin of the decrease in A_{rel} and $\langle H \rangle$ in figures 3(a) and (b), respectively.

Even though the overall amorphous content A_{rel} is falling, the number of Fe atoms which have mostly Nb, Cu and possibly some B atoms as their nearest neighbours and which are represented by the low-field hump is rising. This behaviour is seen better in figure 5 for $x = 1.5$. In figure 4 the decrease at 16 h is only apparent because we have to take the mutual ratio of the low-field to the high-field peak into account. In this case even the close-to-zero field values are increasing. Moreover, the overall intergranular phase is strongly reduced as seen in figure 3(a) (open circles).

The increasing importance of Fe atoms surrounded by Nb, Cu and B is explained by the poor solubility of these elements in the $D0_3$ Fe–Si alloy [4] which, in turn, leads to their clustering. Consequently, the following effects are observed:

(i) the average hyperfine field is decreased as seen in figure 3(b)
(ii) the standard deviation in figure 3(c) is increased.

The latter can be interpreted as due to qualitative changes in the short-range order of both chemical and topological origin which give rise to the formation of new surroundings of the resonant atoms. As a result, changes in the structure, which are represented by the standard deviation, and in the magnetic properties of the residual amorphous phase (reflected through the average field values) are revealed.

The decrease in the field values is demonstrated in figure 4 and 5 by a shift in the maximum high-field hump positions toward lower H values with increasing annealing time. The increase in the Nb content for $x = 1.5$ is also accompanied by changes in the short-range order. This is demonstrated by different positions of the maximum peak values which are situated more to the left than those for the $x = 0$ sample.

4. Conclusion

During the isothermal heat treatment of the amorphous $Fe_{73.5-x}Cu_1Nb_{3+x}Si_{13.5}B_9$ alloy, not only are crystalline grains formed but also the residual amorphous phase undergoes

significant changes. First of all the amount of this phase is reduced with annealing time. The rate of the decrease depends on the Nb content. An increase in x slowed down the crystallization.

Noticeable changes take place in the short-range order of the residual amorphous phase. With progressive crystallization, segregation of Fe, Si and B from the original precursor reduces the number of Fe atoms with high hyperfine fields. As a consequence, the average hyperfine field is falling. On the other hand, those Fe atoms which have mostly Nb, Cu and possibly some B atoms as their nearest neighbours start to dominate. Because their hyperfine fields are rather low, they enhance the above-mentioned effect of the average field reduction.

Changes in the local arrangement of the constituent elements in the residual amorphous phase are also reflected through an increase in the standard deviation. This can be associated with the formation of chemically and topologically new surroundings of the resonant atoms which are created during the annealing.

In order to understand the interesting behaviour of the Fe–Cu–Nb–Si–B nanocrystalline alloys it seems inevitable that the intergranular component should also be studied. In these investigations a crucial role is played by Mössbauer spectroscopy which is able to scan the short-range order arrangement via hyperfine field distributions.

Acknowledgment

The amorphous ribbons were supplied by courtesy of Dr P Duhaj.

References

[1] Herzer G 1992 *J. Magn. Magn. Mater.* **112** 258–62
[2] Gonser U 1991 *Hyperfine Interact.* **68** 71–82
[3] Zemčík T 1993 *Key Eng. Mater.* **81–3** 261–6
[4] Jiang J, Aubertin F, Gonser U and Hilzinger H-R 1991 *Z. Metallk.* **82** 698–702
[5] Hampel G, Pundt A and Hesse J 1992 *J. Phys.: Condens. Matter* **4** 3195–214
[6] Pundt A, Hampel G and Hesse J 1992 *Z. Phys.* B **87** 65–72
[7] Rixecker G, Schaaf P and Gonser U 1992 *J. Phys.: Condens. Matter* **4** 10 295–310
[8] Fujinami M, Hashiguchi Y and Yamamoto T 1990 *Japan. J. Appl. Phys.* **29** L477–80
[9] Makarov V A, Archishevskii M A, Baldokhin U A, Maltsev B I, Zaitcev A J, Sadchikov V V, Ovcharov V P and Sosnin V V 1992 *J. Magn. Magn. Mater.* **112** 290–2
[10] Miglierini M, Lipka J and Sitek J 1993 *Hyperfine Interact.* at press
[11] Petrovič P, Brovko I, Zemčík T, Konč M, Švec T and Dubovinský M 1992 *J. Magn. Magn. Mater.* **112** 331–3
[12] Brovko I, Petrovič P, Zatroch M and Konč M 1993 *Key Eng. Mater.* **81–3** 183–8
[13] Brand R A 1987 *Angewandte Physik, Universität Duisburg* Internal report
[14] Duhaj P, Švec P, Mat'ko I and Janičkovič D 1993 *Key Eng. Mater.* **81–3** 39–48
[15] Zatroch M, Petrovič P and Brovko I 1992 *Nucl. Instrum. Methods* **72** 462–6
[16] Miglierini M, Sitek J, Szász Z and Vitázek K 1993 *Hyperfine Interact.* at press
[17] LeCaër G and Dubois J M 1979 *J. Phys. E: Sci. Instrum.* **12** 1083–90